Body-mounted robotic instrument guide for image-guided cryotherapy of renal cancer

Nobuhiko Hata,[a] Sang-Eun Song, and Olutayo Olubiyi
National Center for Image Guided Therapy, Brigham and Women's Hospital and Harvard Medical School, Boston, Massachusetts 02115

Yasumichi Arimitsu and Kosuke Fujimoto
Mechanics R&D Center, Canon, Inc., Tokyo 146-8501, Japan

Takahisa Kato
Healthcare Optics Research Laboratory, Canon U.S.A., Cambridge, Massachusetts 02144

Kemal Tuncali, Soichiro Tani, and Junichi Tokuda
National Center for Image Guided Therapy, Brigham and Women's Hospital and Harvard Medical School, Boston, Massachusetts 02115

(Received 23 June 2015; revised 10 December 2015; accepted for publication 2 January 2016; published 20 January 2016)

Purpose: Image-guided cryotherapy of renal cancer is an emerging alternative to surgical nephrectomy, particularly for those who cannot sustain the physical burden of surgery. It is well known that the outcome of this therapy depends on the accurate placement of the cryotherapy probe. Therefore, a robotic instrument guide may help physicians aim the cryotherapy probe precisely to maximize the efficacy of the treatment and avoid damage to critical surrounding structures. The objective of this paper was to propose a robotic instrument guide for orienting cryotherapy probes in image-guided cryotherapy of renal cancers. The authors propose a body-mounted robotic guide that is expected to be less susceptible to guidance errors caused by the patient's whole body motion.
Methods: Keeping the device's minimal footprint in mind, the authors developed and validated a body-mounted, robotic instrument guide that can maintain the geometrical relationship between the device and the patient's body, even in the presence of the patient's frequent body motions. The guide can orient the cryotherapy probe with the skin incision point as the remote-center-of-motion. The authors' validation studies included an evaluation of the mechanical accuracy and position repeatability of the robotic instrument guide. The authors also performed a mock MRI-guided cryotherapy procedure with a phantom to compare the advantage of robotically assisted probe replacements over a free-hand approach, by introducing organ motions to investigate their effects on the accurate placement of the cryotherapy probe. Measurements collected for performance analysis included accuracy and time taken for probe placements. Multivariate analysis was performed to assess if either or both organ motion and the robotic guide impacted these measurements.
Results: The mechanical accuracy and position repeatability of the probe placement using the robotic instrument guide were 0.3 and 0.1 mm, respectively, at a depth of 80 mm. The phantom test indicated that the accuracy of probe placement was significantly better with the robotic instrument guide (4.1 mm) than without the guide (6.3 mm, $p < 0.001$), even in the presence of body motion. When independent organ motion was artificially added, in addition to body motion, the advantage of accurate probe placement using the robotic instrument guide disappeared statistically [i.e., 6.0 mm with the robotic guide and 5.9 mm without the robotic guide ($p = 0.906$)]. When the robotic instrument guide was used, the total time required to complete the procedure was reduced from 19.6 to 12.7 min ($p < 0.001$). Multivariable analysis indicated that the robotic instrument guide, not the organ motion, was the cause of statistical significance. The statistical power the authors obtained was 88% in accuracy assessment and 99% higher in duration measurement.
Conclusions: The body-mounted robotic instrument guide allows positioning of the probe during image-guided cryotherapy of renal cancer and was done in fewer attempts and in less time than the free-hand approach. The accuracy of the placement of the cryotherapy probe was better using the robotic instrument guide than without the guide when no organ motion was present. The accuracy between the robotic and free-hand approach becomes comparable when organ motion was present.
 [http://dx.doi.org/10.1118/1.4939875]

Key words: cryotherapy, medical robot, navigation, Magnetic Resonance Imaging, image-guided therapy

1. INTRODUCTION

Frameless stereotactic navigation of interventional instruments for thoracic, abdominal, and pelvic percutaneous interventions enables the interactive visualization of instruments in preoperative and intraoperative images, such as MRI and CT images. Using the navigation system, a physician can plan the trajectory of the tool to reach the lesion precisely, while avoiding unintended injuries to surrounding critical structures. Numerous studies have reported that frameless stereotactic devices cause fewer traumas for patients and provide better outcomes in image-guided interventions.[1] There are several commercial products in this arena as well;[2–7] however, interventionists' use of frameless stereotactic navigation is still quite limited. Some issues that prohibit the prevalence of frameless stereotactic navigation is the inconvenience of placing tool-tracking sensors near the site of the intervention and the lack of an intuitive guide display to assist physicians in placing cryotherapy probes along the desired trajectory. Furthermore, today's frameless stereotactic navigation tools cannot accommodate motions generated by organs or the patient.

One of the emerging solutions that addresses the aforementioned limitations of frameless stereotactic navigation is the use of a robotic instrument guide.[8] These guides can orient tools to the desired trajectory without tool-tracking sensors and without the requirement of the physician's skilled hand-eye coordination in orienting the tool to follow the graphical orientation in the navigation's display. Efforts to develop robotic instruments are underway that use a mounted approach, depending on which surface the robotic instrument guides are placed.[9] The body-mounted systems are attached directly to the patient's skin rather than nearby equipment or the structure of the imaging suite; hence, one can hypothesize that body-mounted robots are less vulnerable to misregistration of guidance images. Furthermore, the body-mounted robot can guide the cryotherapy probe with a relatively simple mechanism that has a smaller footprint compared to other surface-mounted approaches. There has not been, however, much development of body-mounted robotic instrument guides that have been tested or commercialized for application in abdominal and pelvic interventions.[8] Therefore, there is a need and an opportunity to validate the utility of body-mounted robots and review their advantages over frameless stereotactic navigation and other robotic guides.

The objective of this paper was to develop and validate a body-mounted robotic instrument guide for MRI and CT image-guided cryotherapy of renal cancer and validate the accuracy of placing a cryotherapy probe in the presence of organ motion. This work was inspired by the seminal papers authored by Bricault *et al.*[10] and Walsh *et al.*,[11] where a rotational ring base is placed on the patients' abdomen but access to the skin incision site is partially blocked by the arch structures attached to the base ring for probe mobility. As a result, we extended their prior work by proposing a novel two-ring mechanism to increase accessibility to the skin incision site, yet still maintain the mobilization of cryotherapy probes. After the robot was tested in a bench-top study to measure motion accuracy, an additional validation study was performed using a gel phantom in a realistic clinical setting with a MRI scanner mimicking MRI-guided cryotherapy of renal cancer. To differentiate from prior works, we also induced body and organ motions separately to study the impacts of these motions on the accuracy of cryotherapy probe placement.

2. METHODS AND MATERIALS

2.A. Robotic instrument guide

The robotic instrument guide, designed to be placed at the entry point of the cryotherapy probe on the skin, is a physician-controlled device that orients the tool guide to a predefined target (Fig. 1). The robotic instrument guide is comprised of a base stage, a rotary motion stage, and a tool guide assembled on-site on the patient as physicians proceed in image-guided cryotherapy from device registration to probe guidance (Fig. 2). All of the components are designed to sustain the typical ethylene oxide "gas" sterilization cycle. The two ring-shaped rotary stages, stacked on each other with the top stage tilted against the bottom rotary stage, rotate the tool guide independently around the remote-center-of-motion (RCM) fixed at the skin entry point (Fig. 2). In practice, the entry point of the cryotherapy probe and the target is defined prior to the placement of the robotic instrument guide by using a 3D image acquired during the initial stage of the procedure. Afterward, the ring rotary stages align the tool guide to the trajectory defined by the entry and target points.

The tool guide is both detachable and interchangeable to allow various sizes of cryotherapy probes to be used during procedure. These probes can be disposed after use to

FIG. 1. Body-mounted robotic instrument guide: (left) the base mount attachment to large loop containing fiducial markers for device-to-image registration; (right) double ring mechanism with 18-gauge demonstration probe mounted on the base attachment.

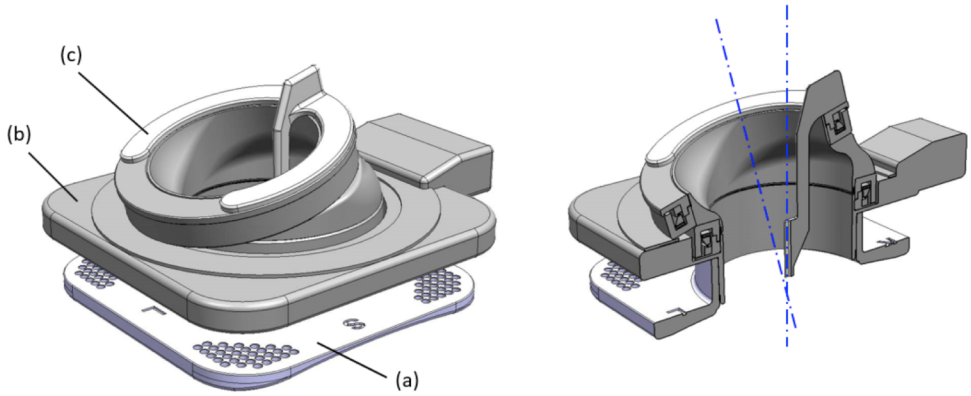

FIG. 2. (Left) Model of the robotic instrument guide: (a) base stage with fiducial markers; (b) top stage with two ring actuation units; (c) detachable instrument guide. The instrument guide is detachable from the rotating units to accommodate multiple probe placements during image-guided cryoablation therapy. (Right) Cross-sectional model: the two axes of rotation created by the two ring-shaped actuation units. (Note that the intersecting point is placed on the bottom center of the device; in clinical applications, this placement will coincide with the skin entry point of the cryoablation probes.)

prevent possible cross-contamination. The guide's hole size was designed to accommodate 18-gauge (outer diameter of 1.3 mm) cryotherapy probes during our validation studies. For the smooth surface finish of the cryotherapy probe contacting area, a 1-mm diameter hole was printed from rapid prototyping, and a 1.4-mm diameter drill hole was created as a postprocess.

Two ring-shaped motor units (Canon, Inc., Tokyo, Japan) were used to actuate the rings of the robot independently. Each of the motor units included an ultrasonic motor and rotary position sensor inside a ring-shaped housing made of polyether ether ketone (PEEK). The unit had an inner diameter of 83 mm, an outer diameter of 111.6 mm, and a thickness of 18 mm. The ultrasonic motor had a ring-shaped vibrator with piezoelectric material and a slider. The slider was oscillated by the piezoelectric material. The resolution of the rotary position sensor was 10 612 pulses per revolution (approximately 2 arc-min).

2.B. Motion control

The two-ring mechanism can be modeled as a serial kinematic chain of two rotary joints for angulation, hereafter referred to as Joint #1 and Joint #2, and a prismatic joint for cryotherapy probe insertion, hereafter referred to as Joint #3. The local coordinate frames for the links were defined according to the Denavit and Hartenberg (DH) convention,[12] where z_1, z_2, and z_3 correspond to the rotational and translational axes of Joints #1, #2, and #3, respectively.

Among the DH parameters of this serial link denoted in Table I and Fig. 3, θ_1, θ_2, d_3 are variables that represent the rotational angles of Joints #1 and #2 and the translational displacement of Joint #3, respectively. The values of α_1 and α_2 are constants that define the angles between the axes of Joints #1 and #2 and between the axes of Joints #2 and #3, respectively. Since the rotational axis of Joint #2 matches that of Joint #1 when $(\theta_1,\theta_2) = (0,\pi)$, α_1 and α_2 must satisfy $\alpha_1 = \alpha_2 \bullet d_2$ which also is a constant value that defines the offset between the origins of the local coordinate frames for Joints #1 and #2. Detailed description of forward and inverse kinematics can be found in the Appendix.

TABLE I. Denavit–Hartenberg link parameters for robotic instrument guide.

i	α_{i-1}	a_{i-1}	d_i	θ_1
1	0	0	0	θ_1[a]
2	α_1	0	d_2	θ_2[a]
3	α_2	0	d_3[a]	0

[a]Joint variable.

2.C. Image guidance software

Image guidance software (Fig. 4) was designed to help physicians perform the following tasks: (1) plan the insertion trajectory of a 3D cryotherapy probe based on the initial MRI interactively; (2) send the planned trajectory to the device's control software; (3) register the robotic instrument guide to

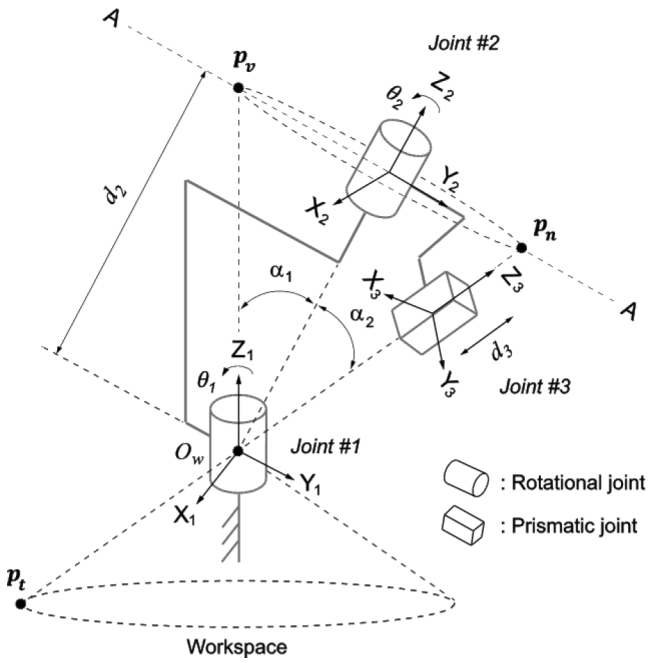

FIG. 3. Model of the two-ring mechanism in Denavit and Hartenberg convention.

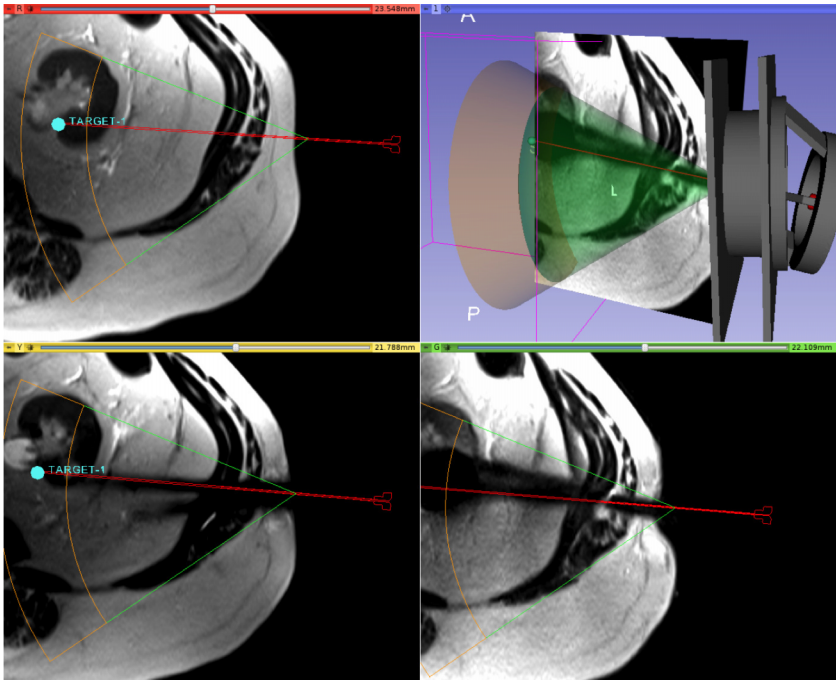

FIG. 4. Screen shot of 3D SLICER navigation software showing the device, workspace, a target position with required projected probe path, and the resulting probe artifact.

the image coordinate frame using the image; (4) confirm the location of the cryotherapy probe on intraprocedural images; and (5) monitor the status of the robotic instrument guide with a 3D model. The image guidance software is implemented as a plug-in extension for free open-source medical image computing software, 3D SLICER,[13] offering various ways of image visualization, including reformatted 2D rendering, volume rendering, and surface rendering. To achieve tasks 2, 4, and 5, the image guidance software communicates with the device control software over the network using the OpenIGTLink protocol.[14]

For task 3, the image guidance software automatically registers the robotic instrument guide to the image coordinate frame by analyzing an intraprocedural image and detecting the fiducial markers attached to the robotic instrument guide with a known configuration. These markers are 3D-printed spherical liquid containers filled with gadoliniumdiethylenetriaminepentacetate (Gd-DTPA) solution and visible in the intraprocedural image. The image is processed by the following steps: First, spherical objects with diameters close to those of the markers are enhanced by the generalized vesselness filter proposed by Frangi *et al.*[15] and segmented by a 3D Hough transform.[16] Then, the center of each sphere is identified. Those filters eliminate other visible structures on the image such as parts of the patient's anatomy. Then, the model of the fiducial frame is matched to the identified centers of the spherical markers, after which the rigid transformation between the model and the identified centers is computed.

2.D. Desktop accuracy study

We evaluated the mechanical accuracy of the robotic instrument guide in terms of consistency in keeping the trajectory on the RCM point and the accuracy of positioning the tip of the cryotherapy probe. A probe-shape stylus was attached to the tool guide with insertion depths of 0 mm (the tip at the RCM point) and 80 mm (the tip at a typical insertion depth of the probe). We commanded the robotic instrument guide to adjust the stylus to 25 target orientations consisting of combinations of five tilt angles from the vertical axis (−30°, −15°, 0°, 15°, and 30°) and five directions about the vertical axis (0°, 36°, 72°, 108°, and 144°). At each target orientation, the distance between the tip of the stylus and the theoretical tip position marked in 3D space in the navigation software was measured using an industrial microscope (MM-800, Nikon, Tokyo, Japan). For each orientation, we repeated the measurements five times. Thus, in total, 250 measurements were made, tabulated, and used to get the average and standard deviation of the measurement values.

2.E. Mock clinical study with simulated organ motion

We performed a phantom validation study to assess the advantages of the robotic instrument guide in terms of time, accuracy of placement of the cryotherapy probe, and number of placement attempts. Virtual locations in the gel phantom that mimicked renal tissue were targeted using the robotic instrument guide in a 3T wide-bore MRI scanner (MAGNETOM Verio 3T, Siemens, Erlangen, Germany). In this study, we used both phantom motion and organ motion to mimic real motions of the patient's body and the patient's organs to investigate the impact of these motions on the aforementioned measurement items. The latter motion was induced by shifting the target point immediately before the probe was placed by a physician. Organ motion was produced after planning so that bias due to correction would be nullified.

A board-certified physician, in general, surgery with five years of experience in percutaneous ablation therapies performed all of the attempts to place the cryotherapy probe.

This mock clinical study was performed in a similar way as image-guided cryotherapy of renal cancer where patients are transferred out of MRI scanners' bore for placement of cryotherapy probes.[17,18] This approach is also referred as an "in and out" approach elsewhere.

Phantoms were created to mimic renal tissue using gelatin (Unflavored Knox Original Gelatine, Kraft Foods, Northfield, IL). The 12% gelatin solution was stirred and placed in a square container with dimensions of approximately $16 \times 16 \times 12.5$ cm. When placing the phantom during the experiment, it was covered with a paper towel to prevent the physician from seeing the trajectory of the cryotherapy probe. The center of the phantom was placed on the MRI table at the same position each time but with random motion of the whole phantom, mimicking the patient's body motion in image-guided therapies. A loop coil (Large Loop Coil, Siemens, Erlangen, Germany) was placed on top of the phantom, and the entire structure was taped to the table to hold it in place. In real clinical applications, the device will be latched to the loop coil using special attachments. The loop coil and the robotic device are then secured to the abdominal wall and the bed using the strip harness in place of the loop coil.

Prior to the insertion of the cryotherapy probe, multislice images were acquired using a half-Fourier acquisition with single-shot turbo spin echo (HASTE) (TR/TE: 1000/200 ms; flip angle: 147°; matrix: 320×190; field of view: 289×340 mm^2; slice thickness: 4 mm) and loaded onto the image guidance software for planning the treatment. Five virtual targets were selected in the image guidance software as points on a renal tumor at which the physician would aim the cryotherapy probe. Three targets were defined on the same image plane at varying depths, while two were placed out of the plane. The overall distribution of the target points was similar to those found in real MRI-guided cryotherapies.

The physician was instructed to aim at the target using an insertion point that was near the center of the phantom with (1) a free-hand approach and (2) the robotic approach. For the free-hand approach, the physician directed and steered the cryotherapy probe toward the target based on prior knowledge of the target location from the planning image. Neither the robotic instrument guide nor the sensors were used in the free-hand approach. For the robotic approach, the robot was first registered to the planning image using the automatic registration described previously. The result was visually inspected by overlaying the 3D surface model onto the MR image. When the robot was not registered well to the planning image, another planning image was acquired for reregistration. The robot was commanded to orient the tool guide to the target where the physician then inserted the cryotherapy probe using the guide. In both approaches, after partial insertion, a multislice confirmation image was acquired using the same parameters as the planning image and transferred to the image guidance software. The physician reviewed the MRI on the image guidance software and decided whether he wanted to remove the cryotherapy probe and reinsert it, attempt to steer the cryotherapy probe, or push the cryotherapy probe deeper. The trial ended when the physician was satisfied with the placement of the tip of the cryotherapy probe in relation to the target.

A set of organ motion was recovered from real MRI-guided percutaneous renal cancer cases performed at Brigham and Women's Hospital (Boston, MA) between May 2013 and August 2014. A total of 216 series of images were collected from 21 cases to recover the motion at 196 time points in the procedures using the first series of images as the reference time point. Data collection and image analysis were approved by the Hospital's Institutional Review Board and conducted under the Health Insurance Portability and Accountability Act (HIPAA) Privacy Rule. The motion of the kidney along right–left, anterior–posterior, and superior–inferior directions was measured by initially registering the reference image series and subsequent image series, followed by visual inspection and manual image alignment, if necessary, to refine the registration. The average movements in the right–left, anterior–posterior, and superior–inferior directions were 0.1, −1.7, and 0.7 mm with standard deviations of 3.1, 3.7, and 4.0 mm, respectively. A Gaussian random number generator was created to output an organ movement in all three directions, which fell within the aforementioned distributions. Without notifying the physicians, organ motion was applied to half of the trials after the physician reviewed and planned the trajectory in the image guidance software and after motion commands had been sent to the probe guidance device in cases of the robotic approach.

2.F. Measurements

We recorded the total number of times the physician decided to re-enter the operating room to change the cryotherapy probe's previous position as the total number of trials. The time for the entire procedure was defined as the time between the initial scan and the finish time, as determined by the physician's satisfaction with the last insertion of the cryotherapy probe.

MR images were reviewed to identify the in-plane distance between the location of the final target and the final position of the tip of the cryotherapy probe. The multiplanar reconstruction view in the PACS viewer (aycan OsiriX PRO, Rochester, NY) was used to identify any cryotherapy probe artifacts in each image. The right–left, anterior–posterior, and superior–inferior coordinates of artifacts of the tip of the cryotherapy probe were recorded to measure the distance from the target and the position of the last position of the tip of the cryotherapy probe for each trial. Using these data, the average distance was calculated for all freehand cases, all robotic cases, freehand cases with and without simulated organ motion, and robotic cases with and without simulated organ motion to better observe the precision with which the cryotherapy probe was placed in both the robotic and freehand methods for inserting the cryotherapy probe.

2.G. Statistical analysis

The data were presented with standard summary statistics. Multivariate analysis was performed to evaluate the effects

TABLE II. Baseline counts and number of insertion attempts by method of probe insertion.

		Insertion method		
		Freehand	Robotic	*p*-value
All				
	Single trial	13	24	
	Multiple trials	17	6	0.003
No organ motion				
	Single trial	9	14	
	Multiple trials	6	1	0.031
Organ motion				
	Single trial	4	10	
	Multiple trials	11	5	0.028

of the methods of insertion, application of organ motion, and number of insertion attempts on both the cryotherapy probe placement error and the duration of the procedure. Additional statistical assessments were performed to identify the causes of lengthening (shortening) the duration of procedure and decreasing (increasing) the accuracy of the placement of the cryotherapy probe. This was done by multivariate analysis. Only *p*-values were reported, and *p*-values of 0.05 or less were considered to be statistically significant. All statistical analyzes were performed using STATA version 11.2 (StataCorp LP 2009, College Station, TX).

3. EXPERIMENTAL RESULTS

3.A. Mechanical accuracy study

Maximum absolute positioning error was 0.2 mm at the RCM point, and it was 0.3 mm at the depth of 80 mm under the RCM point. Positioning repeatability was 0.1 mm at the RCM point and 0.1 mm at a depth of 80 mm under the RCM point.

3.B. Placement of the cryotherapy probe with simulated organ motion

Out of the 60 insertions of the cryotherapy probe, 30 were performed free-handedly, and 30 were performed robotically. Fifty percent or 15 trials of each group were performed when simulated organ motion was occurring. The mean value of organ motion that was applied was 5.4 ± 2.6 mm for freehand insertions and 5.8 ± 2.6 mm for robotic insertions, with no statistically significant differences in the two groups. All 60 trials included body (or phantom) motions.

Among 30 probe insertions performed robotically, the robot was successfully registered to the images in 29; in one insertion, the registration initially failed, but successfully registered after reacquiring the second image. The average fiducial registration error was approximately 1.5 mm. The computation time for the registration was approximately 30 s.

Satisfactory placement of the tip of the cryotherapy probe in a single attempt occurred in 13 freehand insertions and in 24 robotic insertions, with a statistical difference of $p = 0.003$ between the two types of insertions (Table II). This significance existed even after introducing organ motions, with $p = 0.028$. In summary, the robotic method required less insertion attempts irrespective of the presence of organ motion. These analyses have estimated statistical power of 88% and higher.

The overall mean error of probe placement was 5.2 mm, but it was significantly smaller for the robotic insertions (4.1 mm) than the freehand insertions (6.3 mm), with $p < 0.001$, when body motion was introduced but without organ motion (Table III). Figure 5 shows typical images obtained in freehand and robot-guided placements of the cryotherapy probe. The advantage of more accurate robotic insertions no longer existed after the introduction of organ motion, $p = 0.906$, as depicted in Fig. 6. Images of both

TABLE III. Summary of applied offsets, duration of procedure, and error of probe tip placement.

Variable		Category	Count	Mean ± SD	Range	*p*-values
Accuracy (mm)						
	All		60	5.2 ± 2.6	14.0–7.0	
		Freehand	30	6.3 ± 3.1	1.6–12.4	
		Robotic	30	4.1 ± 3.1	0.5–12.8	0.008
	No organ motion					
		Freehand	15	6.6 ± 3.1	4.9–8.3	
		Robotic	15	2.1 ± 1.3	1.3–2.8	<0.001
	Organ motion					
		Freehand	15	5.9 ± 3.2	4.1–7.7	
		Robotic	15	6.0 ± 3.1	4.3–7.7	0.9
Total duration (min)						
	All		60	16.2 ± 6.2	10–41	
		Freehand	30	19.6 ± 7.0	12–41	
		Robotic	30	12.7 ± 2.4	10–19	<0.001
	No organ motion					
		Freehand	15	18.7 ± 5.2	15.9–21.6	
		Robotic	15	11.9 ± 1.9	10.8–12.9	<0.001
	Organ motion					
		Freehand	15	20.5 ± 8.5	15.8–25.3	
		Robotic	15	14.0 ± 2.8	12.5–15.5	0.009

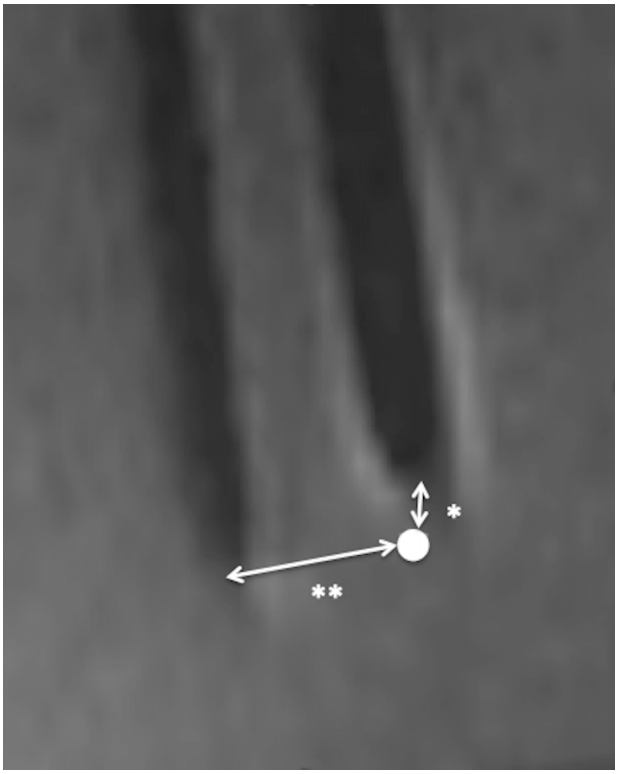

FIG. 5. Highlighted MR images from robotic and free-hand probe placement overplayed to present inserted cryoablation probes aiming at a target (white circle) placed approximately 80 mm from the surface of the gel phantom. The phantom and the body-mounted robotic instrument guide were moved during insertion attempts, but no organ motion was introduced in the trial. Note that the robotic instrument guide can orient the probe with an accuracy of 2.0 mm (one star), while the manual approach produced an accuracy of 6.5 mm (two stars) from the target.

the free-hand approach and robotic guide contain fiducial markers from the device. These markings register the robot to the image, where the user can go on to determine the probe target. With this information, we are able to determine the trajectory path the device took to guide the probe into the patient. Given the limitations of the device, there is a restricted range of motion that the probe is allowed to travel. Any coordinates that do not agree with this restriction can be considered done during the free-hand approach.

TABLE IV. Impact of multivariate analysis, $n = 60$.

Variables		Coefficient	p-value	[95% conf. interval]
Total duration (power > 99%)				
	Organ motion	−0.1	0.9	−1.6 to 1.5
	Robotic	−2.3	0.008	−4.1 to −0.6
Accuracy (power = 88%)				
	Organ motion	1.8	0.03	0.2–3.4
	Robotic	−2.5	0.006	−4.3 to −0.8

The average duration of the procedure was 16.2 min; the duration of procedures was significantly shorter in the robotic approach (12.7 min) than in the freehand approach (19.6 min), with $p < 0.001$. The durations remained significantly different even with the introduction of motion (offset), $p = 0.009$ (Table III). Table III also indicates that the duration of the procedure was reduced and the accuracy of the placements of the cryotherapy probe was increased, while using the robotic instrument guide ($p < 0.001$ and $p = 0.008$, respectively). Organ motion impacted the accuracy of the placement of the cryotherapy probe, but it had less impact on the duration of probe placements (Table IV). The use of the robotic guide improved the duration and accuracy of the probe placement at statistically significant levels. Time required for the device setup was not counted in the study; however, we estimate that the placement of the robot on the RF coil takes approximately 5–10 min. before the procedure, offsetting some of the advantages of faster probe placement using the guide device.

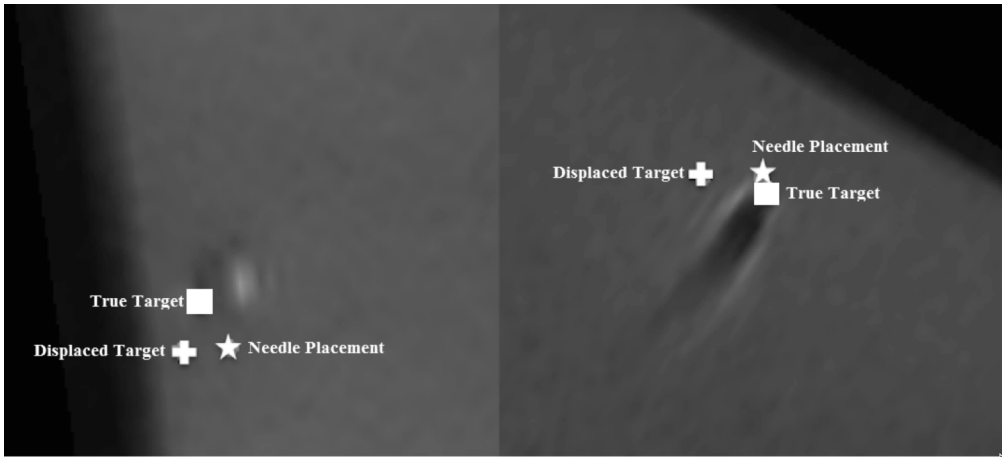

FIG. 6. Highlighted MR images from free-hand (left) and robotic (right) probe placements. The tip of the probe artifact (marked as "Needle Placement" with white star) in both images. Note the true target ("True Target" with white square) is aimed more precisely in the robotic approach than in the free-hand approach, compared to when the target shifted due to artificial organ motion ("Displaced Target" with white plus) which is missed by both approaches by similar degree of distance.

4. DISCUSSION AND CONCLUSIONS

We presented a body-mounted robotic instrument guide for image-guided cryotherapy of renal cancer in an attempt to facilitate accurate placement of the cryotherapy probe on cancerous lesions. We found that the robotic instrument guide allowed faster placement with fewer placement attempts when compared to the freehand approach, irrespective of the presence of organ motion. The accuracy of the placement of the cryotherapy probe was enhanced by the use of the robotic instrument guide when no organ motion was occurring, and the two techniques were comparable when organ motion was occurring. Multivariate analysis showed that the robotic instrument guide had a significant impact on the total duration of the procedure and the accuracy of the placement of the cryotherapy probe. This study demonstrates the advantage of using a body-mounted robot to place cryotherapy probes in the presence of body motion and organ motion by comparing the robotic and manual approaches.

The findings from our study are analogous to other robotic instrument guides that compare freehand and robotic instrument guides. Tilak *et al.*[19] reported that, in their comparison of robotic and freehand insertions of the biopsy probe in MRI-guided prostate biopsies, the robotic instrument guide made the procedure faster and more accurate. The impact of organ motion was not addressed in their study. Likewise, Boctor *et al.*[20] presented the advantage of a robotic instrument guide in the ultrasound-guided placement of percutaneous cryotherapy probes (1.6 vs 3.2 mm). In addition, breast biopsies were improved by a mechanical tool guide developed by Bluvol *et al.*[21] The latter study and ours were comparable with respect to the effect of motion in that the inclusion of heartbeat and respiratory effects increased the placement error to 5.5 mm.

Our study did not include an image compatibility test to quantify the MRI and CT compatibility of the robotic instrument guide. The guide was developed in accordance with the design strategy of a MRI-compatible robot that is commonly found in the literature studies from the authors' group.[22,23] In fact, our casual assessment of the image quality with the robotic instrument guide during imaging in CT and MRI showed no significant degradation of either images. The intended use of the robotic instrument guide in the current form does not include actuation of ultrasonic motors in the MRI or CT scanner. Therefore, our concern for MRI-compatibility and CT-compatibility was focused mostly on the safe and robust operation of the encoder during imaging, but there was no evident degradation of the operation of the encoder operation during the experiments. Further analysis is required for the continued safe operation of the robotic instrument guide. The study is also limited that we used image artifact of the probes in MR images, not physical measurement, to localize the probes in our accuracy studies. Although use of MRI for assessing probe placement accuracy is common,[24] it is also well known that probe artifact does not represent the location of the probe accurately,[25,26] especially so when frequency encoding direction of the imaging is perpendicular to the probe shaft. It will be desirable to use physical measurement in our future assessment of probe placement accuracy.

Though the robotic guide presented in this paper is primary designed for image-guided cryotherapy of renal cancer, the guide can be extended for other application as well. An example of other applications that may be benefited from the use of the robotic guides is image-guided tumor ablations of lung, liver, bone, or even extrahepatic, extrarenal, intra-abdominal cancers. The device is expected to be more useful when the body motion invalidates the planning based on prior images, causing error in applicator placements.

The robotic instrument guide is also expected to provide several clinical benefits in tumor diagnosis by enabling precision biopsies. Two examples are given below to justify the use of such a precise instrument guide. Although tumors may be similar in overall morphology, they may differ in their oncogenic drivers' and responses to the same therapies.[27] As oncology management advances toward precision medicine, in which such oncogenic drivers are identified and corresponding drugs are administered, it is essential that image-guided biopsies capture the molecular heterogeneity of tumors, particularly intratumoral heterogeneity.[28,29] A robotic instrument guide assisted by advanced biomarker imaging can place biopsy needles at different tumor sites with different molecular and genomic states. The comprehensive molecular and genetic diagnosis of each cancer can be used to administer the right combination of drugs to the patient. Such precise biopsies can be repeated throughout the treatment by monitoring the progression of molecular and genetic changes in the site over time.

The current study confirmed that the accuracy of the placement of the cryotherapy probe was comparable in both the robotic and manual approaches when organ motion was occurring. The organ motion in general is controlled well in standard practice of image-guided therapies as is indicated in a paper.[30] Most of the freehand image-guided navigation methods available commercially and academically have been used under the assumption that the organ motion is controlled in standard clinical approaches. The current study however revealed that the organ motion indeed limits the benefit of navigated or robotic guidance. Further study is warranted to handle the organ motion in both navigated and robotically guided cryoablation therapies.

Clinical advantage of the current robotic system is not yet to be proven but warrants further examination. The possibility of studies to assess benefits of the robot may measure usability of the robot, ease or difficulty of adopting the robot, and skills and knowledge required to use the robot effectively. Future study may also assess if a robot can extend the indication for the image-guided renal cancer itself. The literature suggests that the image-guided cryoablation (or ablation in general) is limited to renal masses of 4 cm or smaller[31] primarily due to difficulty to optimally place ablation probes to cover larger tumors. The current device can be used to address this challenge by helping physicians to optimally and precisely place ablation probes to treat larger tumors.

In 2015, approximately 61 000 new cases of kidney cancer are likely to occur. In fact, the incidence of detecting renal cancer is increasing presumably due to the advancement of abdominal imaging. Studies have shown that minimally invasive therapies, such as laparoscopic partial nephrectomy, can offer better overall survival with a prognosis that is equivalent to that of radical nephrectomy.[29] Minimally invasive therapies are particularly appealing to patients with small renal cancers, because their goals for treatment are to cure the cancer and preserve the renal function. Image-guided cryotherapy of renal cancer is emerging as a strong alternative to laparoscopic partial nephrectomy, especially for patients who already have undergone renal surgery or patients who are medically unfit for invasive surgical procedures.[17,18] During renal cryotherapy, an interventional radiologist aims a thin, probe-like cryotherapy probe percutaneously into the tumor, under MRI or CT guidance. However, it is well known that the success of renal cryotherapy depends heavily on the precise and accurate placement of the cryotherapy probes into the tumor while avoiding critical health structures.[32,33] Our future study is expected to show that a robotic instrument guide and image guidance software can help physicians perform image-guided cryotherapy for renal cancer with precision, confidence, and in less time.

The use of the robotic instrument guide may, however, introduce additional challenges to the image-guided cryotherapies. First, the device will occupy the physicians workplace near insertion site and limit the freedom of maneuvering ablation applicators, or performing minor surgical care near the incision site. We believe that this concern on limited workspace is partially resolved by our unique double-ring mechanism to secure the hollow open space within the device allowing physicians to put their hands through it in order to reach the incision site. However, additional clinical validation study is necessary to confirm that our design produces enough space for physicians. Our study indicated that the usefulness of our device is not impacted by body motion; however, the organ motion remains to be an obstacle in image-guided therapy, in general, and our device was not yet capable of addressing this general issue. We are considering the addition of organ tracking methods to improve the accuracy of probe placement, using our prior work.[34,35]

In conclusion, we have demonstrated that the body-mounted robotic instrument guide facilitated accurate and faster placement of the cryotherapy probe in image-guided cryotherapy of renal cancer, yet the advantage of robotic-guided placement of the cryotherapy probe diminishes in the presence of organ motion. Further development to handle organ motion in the body-mounted robot is needed.

ACKNOWLEDGMENTS

The authors gratefully acknowledge Laurent Chauvin, Brian Ninni, Kazufumi Onuma, Kenichi Kataoka, Jae Hee Park, and Peter Tia for their technical assistance and Duy Doan and Christopher Blanchard for editorial assistance. Research reported in this publication was supported by Canon USA, Inc., and The National Institute of Biomedical Imaging and Bioengineering of the National Institutes of Health under Award No. P41EB015898. The content is solely the responsibility of the authors and does not necessarily represent the official views of the National Institutes of Health. N.H. is a member of the Board of Directors of Mebio, Inc., and has an equity interest in the company. N.H.'s interests were reviewed and are managed by the Brigham and Women's Hospital and Partners HealthCare in accordance with their conflict of interest policies. Y.A. and K.F. are employees of Canon, Inc., and T.K. is an employee of Canon USA, Inc. Canon, Inc., provided the actuators for this study and Canon USA, Inc., partially funded this study.

APPENDIX: KINEMATICS

Using the convention depicted in Fig. 3, the transformation matrix from the device's coordinate frame to the coordinate frame for Joint #3, ${}^{0}_{3}T$ can be described as

$$ {}^{0}_{3}T = {}^{0}_{1}T\,{}^{1}_{2}T\,{}^{2}_{3}T, \tag{A1} $$

where ${}^{0}_{1}T$, ${}^{1}_{2}T$, and ${}^{2}_{3}T$ are the DH matrices for the transformations associated with Joints #1, #2, and #3, respectively. ${}^{0}_{1}T$, ${}^{1}_{2}T$, and ${}^{2}_{3}T$ can be described as

$$ {}^{0}_{1}T = \begin{bmatrix} \cos\theta_1 & -\sin\theta_1 & 0 & 0 \\ \sin\theta_1 & \cos\theta_1 & 0 & 0 \\ 0 & 0 & 1 & 0 \\ 0 & 0 & 0 & 1 \end{bmatrix}, \tag{A2} $$

$$ {}^{1}_{2}T = \begin{bmatrix} \cos\theta_2 & -\sin\theta_2\sin\alpha_1 & \sin\theta_2\sin\alpha_1 & 0 \\ \sin\theta_2 & \cos\theta_2\cos\alpha_1 & -\cos\theta_2\sin\alpha_1 & 0 \\ 0 & \sin\alpha_1 & \cos\alpha_1 & d_2 \\ 0 & 0 & 0 & 1 \end{bmatrix}, \tag{A3} $$

$$ {}^{2}_{3}T = \begin{bmatrix} 1 & 0 & 0 & 0 \\ 0 & \cos\alpha_2 & -\sin\alpha_2 & 0 \\ 0 & \sin\alpha_2 & \cos\alpha_2 & d_3 \\ 0 & 0 & 0 & 1 \end{bmatrix}. \tag{A4} $$

The inverse kinematics of the mechanism can be solved geometrically. In Fig. 7, O_w denotes the origin of the device's coordinate system, and p_n denotes position at which the cryotherapy probe was inserted on the small ring. In addition, p_v is a reference position to be used in the inverse kinematic calculation, at which the axis of the lower ring passes through the upper ring. Once the robotic instrument guide is placed at a desired position, O_w coincides with the RCM. When a target p_t is given, the cryotherapy probe insertion path is obtained as a line that connects the target p_t and O_w. Since this line passes through p_n and the distance between O_D and p_n is given by the design parameters, α_2 and d_2, the cryotherapy probe insertion position p_n can be obtained as

$$ p_n = \frac{p_t}{|p_t|}(d_2/\cos\alpha_2). \tag{A5} $$

With the known reference position, p_v, the three joint variables, i.e., θ_1, θ_2, and d_3, can now be calculated inversely.

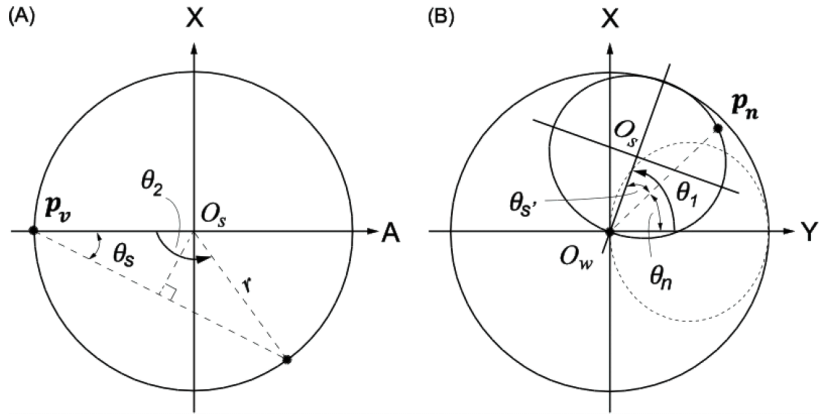

FIG. 7. (A) Kinematic structure of the small ring on its plane: O_s, θ_2, and θ_s are the center, required small ring angle, and offset angle, respectively. P_v is the vertical tip position of the small ring, and p_n is the point on the small ring that is on the planned cryotherapy probe path. (B) Overall kinematic structure. A solid line on the small ring represents the position to create the planned cryotherapy probe path. The dotted line represents an initial position of the small ring. $\theta_{s'}$ and θ_n are the tilted offset angle and insertion position angle from p_n, respectively.

Figure 7 illustrates the kinematic structure of the upper ring on its plane and that of both rings on a global coordinate system, respectively. First, the required upper ring rotation, θ_2, that provides the tilt angle at which the cryotherapy probe is to be inserted can be calculated using the geometry of an isosceles triangle as follows:

$$\theta_2 = \pm 2\sin^{-1}\left(\frac{|p_n - p_v|}{2r}\right), \tag{A6}$$

where r is the radius of the upper ring obtained from the design parameters α_2 and d_2 as

$$r = d_2 \tan \alpha_2. \tag{A7}$$

Because of the nondirectional tilt angling of the upper ring, two kinematic solutions exist for a single tilt angle, except zero and the maximum tilt angle.

Once the tilt angle θ_2 is obtained, the required rotation of the lower ring (i.e., coronal direction of the insertion of the cryotherapy probe) θ_1 can be calculated by adding the tilted offset angle $\theta_{s'}$ to the required angle for the position of the insertion of the cryotherapy probe p_n on the global coordinate θ_n, as shown in Fig. 5. From a given position, $p_n = (x_n, y_n, z_n)$, θ_1 can be calculated as

$$\theta_1 = \tan^{-1}\left(\frac{y_n}{x_n}\right) + \sin^{-1}\frac{\sin\theta_2 |p_n - p_v|}{\sqrt{({y_n}^2 + {x_n}^2)}}, \tag{A8}$$

where $x_n = y_n = 0$, and θ_1 can be any angle; when $x_n = 0$, the first term becomes $\pi/2$ ($y_n > 0$) or $3\pi/2$ ($y_n < 0$).

The required insertion depth of the cryotherapy probe, d, can be obtained by simply calculating the distance between the target and the insertion position of the cryotherapy probe,

$$d = |p_n - p_t|. \tag{A9}$$

[a]Electronic mail: hata@bwh.harvard.edu; http://snr.spl.harvard.edu/.

[1]F. Banovac, J. Tang, S. Xu, D. Lindisch, H. Y. Chung, E. B. Levy, T. Chang, M. F. McCullough, Z. Yaniv, B. J. Wood, and K. Cleary, "Precision targeting of liver lesions using a novel electromagnetic navigation device in physiologic phantom and swine," Med. Phys. **32**, 2698–2705 (2005).

[2]J. Krucker, S. Xu, N. Glossop, A. Viswanathan, J. Borgert, H. Schulz, and B. J. Wood, "Electromagnetic tracking for thermal ablation and biopsy guidance: Clinical evaluation of spatial accuracy," J. Vasc. Interv. Radiol. **18**, 1141–1150 (2007).

[3]E. B. Levy, J. Tang, D. Lindisch, N. Glossop, F. Banovac, and K. Cleary, "Implementation of an electromagnetic tracking system for accurate intrahepatic puncture needle guidance: Accuracy results in an *in vitro* model," Acad. Radiol. **14**, 344–354 (2007).

[4]L. Maier-Hein, A. Tekbas, A. Seitel, F. Pianka, S. A. Muller, S. Satzl, S. Schawo, B. Radeleff, R. Tetzlaff, A. M. Franz, B. P. Muller-Stich, I. Wolf, H. U. Kauczor, B. M. Schmied, and H. P. Meinzer, "*In vivo* accuracy assessment of a needle-based navigation system for CT-guided radiofrequency ablation of the liver," Med. Phys. **35**, 5385–5396 (2008).

[5]B. J. Wood, H. Zhang, A. Durrani, N. Glossop, S. Ranjan, D. Lindisch, E. Levy, F. Banovac, J. Borgert, S. Krueger, J. Kruecker, A. Viswanathan, and K. Cleary, "Navigation with electromagnetic tracking for interventional radiology procedures: A feasibility study," J. Vasc. Interv. Radiol. **16**, 493–505 (2005).

[6]B. C. Meyer, O. Peter, M. Nagel, M. Hoheisel, B. B. Frericks, K. J. Wolf, and F. K. Wacker, "Electromagnetic field-based navigation for percutaneous punctures on C-arm CT: Experimental evaluation and clinical application," Eur. Radiol. **18**, 2855–2864 (2008).

[7]A. M. Palestrant, "Comprehensive approach to CT-guided procedures with a hand-held guidance device," Radiology **174**, 270–272 (1990).

[8]J. Kettenbach and G. Kronreif, "Robotic systems for percutaneous needle-guided interventions," Minimally Invasive Ther. Allied Technol. **24**, 45–53 (2015).

[9]M. M. Arnolli, N. C. Hanumara, M. Franken, D. M. Brouwer, and I. A. M. J. Broeders, "An overview of systems for CT- and MRI-guided percutaneous needle placement in the thorax and abdomen," Int. J. Med. Rob. Comput. Assisted Surg. **11**, 458–475 (2014).

[10]I. Bricault, N. Zemiti, E. Jouniaux, C. Fouard, E. Taillant, F. Dorandeu, and P. Cinquin, "Light puncture robot for CT and MRI interventions: Designing a new robotic architecture to perform abdominal and thoracic punctures," IEEE Eng. Med. Biol. Mag. **27**, 42–50 (2008).

[11]C. J. Walsh, N. C. Hanumara, A. H. Slocum, J.-A. Shepard, and R. Gupta, "A patient-mounted, telerobotic tool for CT-guided percutaneous interventions," J. Med. Devices **2**, 011007 (2008).

[12]J. Denavit and R. S. Hartenberg, "A kinematic notation for lower-pair mechanisms based on matrices," Trans. ASME J. Appl. Mech. **23**, 215–221 (1955).

[13]S. A. Gering, M. A. Foster, M. C. Harnisch, and J. J. McNeil, "Traumatic pneumobilia: Case report," J. Trauma **51**, 391–394 (2001).

[14]J. Tokuda, G. S. Fischer, X. Papademetris, Z. Yaniv, L. Ibanez, P. Cheng, H. Liu, J. Blevins, J. Arata, A. J. Golby, T. Kapur, S. Pieper, E. C. Burdette, G. Fichtinger, C. M. Tempany, and N. Hata, "Openigtlink: An open network protocol for image-guided therapy environment," Int. J. Med. Rob. Comput. Assisted Surg. **5**, 423–434 (2009).

[15]A. Frangi, W. Niessen, K. Vincken, and M. Viergever, "Multiscale vessel enhancement filtering," in *Medical Image Computing and Computer-*

Assisted Interventation—MICCAI'98 , Lecture Notes in Computer Science, edited by W. Wells, A. Colchester, and S. Delp (Springer, Berlin, Heidelberg, 1998) Vol. 1496, pp. 130–137.
[16]R. O. Duda and P. E. Hart, "Use of the Hough transformation to detect lines and curves in pictures," Commun. ACM **15**, 11–15 (1972).
[17]A. Gupta, M. E. Allaf, L. R. Kavoussi, T. W. Jarrett, D. Y. Chan, L. M. Su, and S. B. Solomon, "Computerized tomography guided percutaneous renal cryoablation with the patient under conscious sedation: Initial clinical experience," J. Urol. **175**, 447–452 (2006), discussion 452–453.
[18]K. Tuncali, P. R. Morrison, C. S. Winalski, J. A. Carrino, S. Shankar, J. E. Ready, E. vanSonnenberg, and S. G. Silverman, "MRI-guided percutaneous cryotherapy for soft-tissue and bone metastases: Initial experience," AJR, Am. J. Roentgenol. **189**, 232–239 (2007).
[19]G. Tilak, K. Tuncali, S. E. Song, J. Tokuda, O. Olubiyi, F. Fennessy, A. Fedorov, T. Penzkofer, C. Tempany, and N. Hata, "3T MR-guided in-bore transperineal prostate biopsy: A comparison of robotic and manual needle-guidance templates," J. Magn. Reson. Imaging **42**, 63–71 (2014).
[20]E. M. Boctor, M. A. Choti, E. C. Burdette, and R. J. Webster III, "Three-dimensional ultrasound-guided robotic needle placement: An experimental evaluation," Int. J. Med. Rob. Comput. Assisted Surg. **4**, 180–191 (2008).
[21]N. Bluvol, A. Kornecki, A. Shaikh, D. Del Rey Fernandez, D. H. Taves, and A. Fenster, "Freehand versus guided breast biopsy: Comparison of accuracy, needle motion, and biopsy time in a tissue model," AJR, Am. J. Roentgenol. **192**, 1720–1725 (2009).
[22]N. Hata, J. Tokuda, S. Hurwitz, and S. Morikawa, "MRI-compatible manipulator with remote-center-of-motion control," J. Magn. Reson. Imaging **27**, 1130–1138 (2008).
[23]S. E. Song, J. Tokuda, K. Tuncali, C. M. Tempany, E. Zhang, and N. Hata, "Development and preliminary evaluation of a motorized needle guide template for MRI-guided targeted prostate biopsy," IEEE Trans. Biomed. Eng. **60**, 3019–3027 (2013).
[24]P. Blumenfeld, N. Hata, S. DiMaio, K. Zou, S. Haker, G. Fichtinger, and C. M. C. Tempany, "Transperineal prostate biopsy under magnetic resonance image guidance: A needle placement accuracy study," J. Magn. Reson. Imaging **26**, 688–694 (2007).
[25]J. S. Lewin, J. L. Duerk, V. R. Jain, C. A. Petersilge, C. P. Chao, and J. R. Haaga, "Needle localization in MR-guided biopsy and aspiration: Effects of field strength, sequence design, and magnetic field orientation," AJR, Am. J. Roentgenol. **166**, 1337–1345 (1996).
[26]S. P. DiMaio, D. F. Kacher, R. E. Ellis, G. Fichtinger, N. Hata, G. P. Zientara, L. P. Panych, R. Kikinis, and F. A. Jolesz, "Needle artifact localization in 3T MR images," Stud. Health Technol. Inf. **119**, 120–125 (2006).
[27]V. Nair, S. E. Fischer, and O. A. Adeyi, "Non-viral-related pathologic findings in liver needle biopsy specimens from patients with chronic viral hepatitis," Am. J. Clin. Pathol. **133**, 127–132 (2010).
[28]B. Vogelstein, N. Papadopoulos, V. E. Velculescu, S. Zhou, L. A. Diaz, and K. W. Kinzler, "Cancer genome landscapes," Science **339**, 1546–1558 (2013).
[29]D. Marshall, J. M. Laberge, B. Firetag, T. Miller, and R. K. Kerlan, "The changing face of percutaneous image-guided biopsy: Molecular profiling and genomic analysis in current practice," J. Vasc. Interv. Radiol. **24**, 1094–1103 (2013).
[30]N. I. Sainani, R. S. Arellano, P. B. Shyn, D. A. Gervais, P. R. Mueller, and S. G. Silverman, "The challenging image-guided abdominal mass biopsy: Established and emerging techniques 'if you can see it, you can biopsy it,'" Abdom. Imaging **38**, 672–696 (2013).
[31]D. A. Gervais, F. J. McGovern, R. S. Arellano, W. S. McDougal, and P. R. Mueller, "Radiofrequency ablation of renal cell carcinoma: Part 1, indications, results, and role in patient management over a 6-year period and ablation of 100 tumors," AJR, Am. J. Roentgenol. **185**, 64–71 (2005).
[32]S. Permpongkosol, R. E. Link, L. R. Kavoussi, and S. B. Solomon, "Percutaneous computerized tomography guided cryoablation for localized renal cell carcinoma: Factors influencing success," J. Urol. **176**, 1963–1968 (2006), discussion 1968.
[33]G. D. Schmit, T. D. Atwell, B. C. Leibovich, M. R. Callstrom, A. N. Kurup, D. A. Woodrum, and J. W. Charboneau, "Percutaneous cryoablation of anterior renal masses: Technique, efficacy, and safety," AJR, Am. J. Roentgenol. **195**, 1418–1422 (2010).
[34]J. Tokuda, S. Morikawa, T. Dohi, and N. Hata, "Motion tracking in MR-guided liver therapy by using navigator echoes and projection profile matching," Acad. Radiol. **11**, 111–120 (2004).
[35]J. Lesniak, J. Tokuda, R. Kikinis, C. Burghart, and N. Hata, "A device guidance method for organ motion compensation in MRI-guided therapy," Phys. Med. Biol. **52**, 6427–6438 (2007).